

# Isotropic vs. Anisotropic components of BAO data: a tool for model selection

**Balakrishna S. Haridasu**<sup>a,b,c</sup> **Vladimir V. Luković**<sup>b,c</sup> **Nicola Vittorio**<sup>b,c</sup>

<sup>a</sup>Gran Sasso Science Institute , Viale Francesco Crispi 7, I-67100 L'Aquila, Italy

<sup>b</sup>Dipartimento di Fisica, Università di Roma "Tor Vergata", Via della Ricerca Scientifica 1, I-00133, Roma, Italy

<sup>c</sup>Sezione INFN, Università di Roma "Tor Vergata", Via della Ricerca Scientifica 1, I-00133, Roma, Italy

E-mail: [sandeep.haridasu@gssi.it](mailto:sandeep.haridasu@gssi.it), [vladimir.lukovic@roma2.infn.it](mailto:vladimir.lukovic@roma2.infn.it),  
[nicola.vittorio@roma2.infn.it](mailto:nicola.vittorio@roma2.infn.it)

**Abstract.** We conduct a selective analysis of the isotropic ( $D_V$ ) and anisotropic ( $AP$ ) components of the most recent Baryon Acoustic Oscillations (BAO) data. We find that these components provide significantly different constraints and could provide strong diagnostics for model selection, also in view of more precise data to arrive. For instance, in the  $\Lambda$ CDM model, we find a mild tension of  $\sim 2\sigma$  for the  $\Omega_m$  estimates obtained using  $D_V$  and  $AP$  separately. Considering both  $\Omega_k$  and  $w$  as free parameters, we find that the concordance model is in tension with the best-fit values provided by the BAO data alone at  $2.2\sigma$ . We complemented the BAO data with the Supernova Ia (SNIa) and Observational *Hubble* datasets to perform a joint analysis on the  $\Lambda$ CDM model and its standard extensions. By assuming  $\Lambda$ CDM scenario, we find that these data provide  $H_0 = 69.4 \pm 1.7 \text{ km/s Mpc}^{-1}$  as the best-fit value for the present expansion rate. In the  $k\Lambda$ CDM scenario we find that the evidence for acceleration using the BAO data alone is more than  $\sim 5.8\sigma$ , which increases to  $8.4\sigma$  in our joint analysis.

---

## Contents

<b>1</b>	<b>Introduction</b>	<b>1</b>
<b>2</b>	<b>Models</b>	<b>2</b>
<b>3</b>	<b>Data</b>	<b>3</b>
3.1	BAO	4
3.2	OHD and SNIa data	5
<b>4</b>	<b>Results and Discussion</b>	<b>6</b>
4.1	Results from the analysis of BAO data alone	6
4.2	Joint analysis and model selection	9
4.3	Comment on acceleration	11
4.4	Analysis on mock data	12
<b>5</b>	<b>Conclusions</b>	<b>13</b>

---

## 1 Introduction

The Type Ia Supernovae (SNIa) compilation has so far provided the best observational constraints on the cosmological models for the late-time acceleration. At low-redshifts ( $z \lesssim 2$ ), the SNIa [1] constraints were very well complemented by the Observational Hubble parameter (OHD) [2–4] and the Baryon Acoustic Oscillations (BAO) [5, 6].

Cosmological constraints from these low-redshift data were shown to be in a good agreement with those derived from the very precise high-redshift observations of Cosmic Microwave Background (CMB) [7]. As a result, the  $\Lambda$ CDM model has clearly emerged as the “concordance model” [8–10]. However, several questions have been raised regarding a concordance value for the  $H_0$  [11–13]. It has been shown time and again that the  $H_0$  value from the direct estimate has been in a possible tension with the indirect model-dependent estimate. The more recent direct estimate [11] provides  $H_0 = (73.24 \pm 1.74)$  km/s Mpc $^{-1}$  (hereafter R16)<sup>1</sup>, while the Planck collaboration [15] derived  $H_0 = (66.93 \pm 0.62)$  km/s Mpc $^{-1}$  (hereafter P16)<sup>2</sup>. A similar lower value of  $H_0 = 66.98 \pm 1.18$  km/s Mpc $^{-1}$ , has been estimated by including the primordial deuterium abundance to the other datasets [16].

Alongside the tension in the value of  $H_0$ , the current accelerated state of the Universe has also been questioned in [17], which led to a discussion regarding the SNIa analysis and the evidence for a late-time acceleration in [18–21]. More recently, the BAO dataset has been further improved, owing to the precise measurements from the SDSS (DR12) galaxy survey. [6] were able to disentangle the degeneracies in the transverse and the radial components in the redshift range  $0.35 < z < 0.7$ , providing both the transverse comoving distance ( $D_M(z)$ ) and Hubble parameter ( $H(z)$ ). With this improvement, the current BAO data is able to provide stronger constraints among the other low-redshift observations. In fact, using the BAO dataset alone now gives a significant evidence ( $\sim 6.5\sigma$ ) for acceleration [6, 22].

<sup>1</sup>This value has been further revised to  $H_0 = (73.06 \pm 1.76)$  km/s Mpc $^{-1}$  in [14]. However, we refer to R16 in this paper.

<sup>2</sup>See last column of Table 8 in [15].

The earlier measurements of the BAO data were reported for a volume averaged angular diameter distance  $D_V(z)$  [5], which is a one-dimensional isotropic measurement and does not have complete information. In fact, the missing information is contained in the anisotropic component, usually termed as the Alcock-Pazynski parameter  $AP(z)$  [23]. As these two components carry different information from the same observations, using only one of them could lead to biased results and hence incorrect inferences. While the importance of using the anisotropic information is known for many years, in this paper we utilise the newer anisotropic BAO measurements to quantify the differences in the constraints from the isotropic and anisotropic components that can in-turn be used as a substantial method for falsifying models. We complement the BAO data with SNIa and OHD data to obtain joint constraints on cosmological models and further comment on the issues of  $H_0$  and acceleration. We also show the effects of considering the approximate formulae [8] for the sound horizon at the drag epoch, while testing for the dynamical nature of dark energy.

The paper is organised as follows. In Section 2 the models tested are briefly described. In Section 3 we present the data utilised in this paper, together with a brief description of the method. In Section 4 we report the results of our analysis. Finally, in Section 5 we summarise our findings and discuss our main conclusions.

## 2 Models

In this section we briefly describe the concordance  $\Lambda$ CDM model and its standard extensions that we test and compare in our analysis. The Friedmann equation with all standard degrees of freedom at low-redshifts is given by,

$$H(z)^2 = H_0^2 \left[ \Omega_m (1+z)^3 + \Omega_k (1+z)^2 + \Omega_{DE} f(z) \right], \quad (2.1)$$

where,  $H_0$  is the present expansion rate, while  $\Omega_m$ ,  $\Omega_{DE}$  and  $\Omega_k$  are the dimensionless density parameters of matter, dark energy (DE) and curvature, respectively. The dimensionless density parameters obey the cosmic sum rule of  $\Omega_m + \Omega_{DE} + \Omega_k = 1$ . The general functional form  $f(z)$  gives the evolution of the DE and can be written as,

$$f(z) = \exp \left( 3 \int_0^z \frac{1+w(\xi)}{1+\xi} d\xi \right), \quad (2.2)$$

where  $w(z)$  is the equation of state (EOS) parameter of the dark energy. Hereafter, a constant in redshift EOS parameter is simply represented as  $w$  in contrast to  $w(z)$ . For the flat  $\Lambda$ CDM model,  $\Omega_m = 1 - \Omega_{DE}$  and  $w = -1$ . We test the standard extensions of  $\Lambda$ CDM model, namely the  $k\Lambda$ CDM model with the constraint  $\Omega_m = 1 - \Omega_\Lambda - \Omega_k$ , and the flat  $w$ CDM model with  $w$  as a free parameter. The second Friedmann equation,  $\ddot{a}/a = -4\pi/3G \sum_i \rho_i (1+3w_i)$ , gives us insight into the necessary conditions to be satisfied for assessing the dynamics of expansion rate. The criteria for acceleration can be derived as:  $\Omega_m \leq \Omega_\Lambda/2$  for  $k\Lambda$ CDM and  $w \leq -1/(3\Omega_\Lambda)$  for  $w$ CDM. We can assess the evidence for acceleration by estimating the confidence level at which these criteria are satisfied. One can also derive the deceleration parameter as,

$$q(z) = -a \frac{\ddot{a}}{\dot{a}^2} \equiv (1+z) \frac{H'(z)}{H(z)} - 1. \quad (2.3)$$

A negative value of the deceleration parameter today,  $q(0)$ , implies an expanding universe at an accelerated rate. In addition, one can derive  $q_0 = q(0) = 3/2\Omega_m - \Omega_\Lambda$  for  $\Lambda$ CDM and  $k\Lambda$ CDM models and  $q_0 = 1/2(1+3w(1-\Omega_m))$  for the  $w$ CDM model.

We also study two parameter extensions to  $\Lambda$ CDM, namely  $kw$ CDM and the  $w_0w_a$ CDM. In the former, model both the  $w$  and  $\Omega_k$  are treated as free parameters. The latter model is given by Taylor expanding the EOS parameter around  $a \sim 1$ , as prescribed by the so-called CPL parametrisation [24, 25],

$$w(z) = w_0 + w_a \frac{z}{1+z}. \quad (2.4)$$

The luminosity distance for all these models can be written as,

$$D_L(z) = (1+z) \frac{c}{H_0 \sqrt{|\Omega_k|}} S \left( \sqrt{|\Omega_k|} H_0 \int_0^z \frac{d\xi}{H(\xi)} \right) \quad (2.5)$$

where,

$$S(x) \equiv \begin{cases} \sin(x). & \text{for } \Omega_k < 0 \\ x. & \text{for } \Omega_k = 0 \\ \sinh(x). & \text{for } \Omega_k > 0 \end{cases} \quad (2.6)$$

The theoretical distance modulus is defined as  $\mu_{th} = 5 \log[D_L(\text{Mpc})] + 25$ . The comoving angular diameter distance  $D_M(z)$  is related to  $D_L(z)$  as,

$$D_M(z) = D_L(z)/(1+z), \quad (2.7)$$

which are used in the modelling of BAO data. Alternatively, the other two useful observables in modelling the BAO data are:  $D_V(z)/r_d$  [5] and  $AP(z)$  [23]. The volume averaged comoving angular diameter distance  $D_V(z)$  is given by,

$$D_V(z) = \left[ D_M^2(z) \frac{cz}{H(z)} \right]^{1/3} \quad (2.8)$$

and,  $r_d$  is the sound horizon at the drag epoch ( $z_d$ ) given as,

$$r_d = \int_{z_d}^{\infty} \frac{c_s(z)}{H(z)} dz. \quad (2.9)$$

Recently, in [8], a functional form (hereafter A15) for the estimation of  $r_d$  has been given as

$$r_d = 55.154 \frac{\exp(-72.3(\Omega_b h^2 + 6 \times 10^{-4})^2)}{(\Omega_b h^2)^{0.12807} (\Omega_m h^2 - \Omega_b h^2)^{0.25351}}, \quad (2.10)$$

where  $\Omega_b h^2$  and  $\Omega_b h^2$  are the baryon and neutrino densities, respectively. This functional form has been shown to be accurate up to sub-percent level.

The Alcock-Pazynski parameter was primarily defined as a test for the cosmological constant in [23] and is written as,

$$AP(z) = D_M(z) \frac{H(z)}{c}. \quad (2.11)$$

One can easily construct the observables  $AP(z)$  and  $D_V(z)$  if the measurements for  $D_M(z)$  and  $H(z)$  are available.

### 3 Data

In this section we describe the data used and the different methods adopted to test models against the data. In this current work we use the low-redshift BAO, OHD, and SNIa data.

### 3.1 BAO

The BAO data until recently have been presented for the observable  $D_V(z)/r_d$  [5], owing to the lack of sufficient statistics to distinctly measure  $D_M(z)$  and  $H(z)$ . The  $D_V(z)/r_d$  variable has by far been used to constrain cosmological parameters providing good agreement with the SNIa data [1]. These constraints improve once a joint analysis is performed (e.g., [12]).

In this work we utilise the measurements for  $D_M(z)/r_d$  and  $H(z)r_d$  (hereafter  $D_M\&H$ ) and conduct a selective analysis using the different observables that one can obtain using these measurements. In [6] measurements of  $D_M\&H$  (see their Table 8) at three binned redshifts  $z = 0.32, 0.57, 0.61$  (hereafter 3z)<sup>3</sup> were reported using the galaxy clustering data from Sloan Digital Sky Survey(SDSS) III. Earlier, [26] have presented the observation of the BAO feature at the binned redshift  $z = 2.34$  in the flux-correlation of the Lyman- $\alpha$  forest of high-redshift quasars. Finally, the cross-correlation of Lyman- $\alpha$  forest absorption with the quasars has yielded another measurement at  $z = 2.36$  in [27]. These data points have been updated in [28] and [29], with improvements implemented in their analyses. The newer data points are now given at redshifts  $z = 2.33$  and  $z = 2.4$ . Although, other  $D_V$  measurements at  $z = 0.106, 0.15, 1.52$  [22, 30, 31] are available, we do not implement them in our analysis as the  $AP$  component at their respective redshifts is unavailable.

In [6], the results have also been presented in terms of  $D_V$  and  $AP$  (hereafter  $D_V\&AP$ ) parameter space. Also, the covariance between the  $D_V$  and  $AP$  points is shown to be negligible. Note that, the  $D_V\&AP$  can be derived from the  $D_M\&H$  measurements (see Eq. (2.8)) and then they are equivalent for cosmological parameter estimation. We construct a Jacobian matrix,  $J$ , to propagate the covariance from the  $D_M\&H$  to the isotropic and the anisotropic basis given by  $D_V\&AP$  (see Eq. (3.1)).

$$\Sigma_{D_V\&AP} = J^T \cdot \Sigma_{D_M\&H} \cdot J, \quad (3.1)$$

where  $J$  is defined as the partial derivatives of the final functional form with respect to the initial one. Our formalism of constructing the  $D_V\&AP$  data points converges very well to the covariances already presented in [6]. We implement the same formalism to obtain the  $D_V\&AP$  data points along with their respective correlations for the Lyman- $\alpha$  data points. The correlations between the  $D_M$  and  $H$  estimates are given to be 0.377 and 0.369 at  $z=2.33$  and  $z=2.4$ , respectively [28]. Similarly, we also implement the tomographic BAO data for the 9 redshift bins presented in [32, 33] (hereafter 9z)<sup>3</sup>. The constraints obtained from the 9z data were shown to be more stringent than those using 3z in [10]. For brevity's sake, we show the measurements of  $D_V$  and  $AP$  only for 3z and Lyman- $\alpha$  data in Table 1, and we summarise in Table 2 the covariances for the Lyman- $\alpha$  data points in the  $D_V\&AP$  basis. One can notice the high correlation of the  $D_V$  and  $AP$  points at their respective redshifts. The correlation is found to be  $\sim 0.8$  and  $\sim 0.53$  at redshifts of 2.33 and 2.4, respectively. Given these high correlations, one must always use the full covariance matrix to compare the constraints coming from  $D_M\&H$  with those obtained using  $D_V\&AP$ . Needless to say, this is also true for the 9z data (see also Figure 20 of [32]). Please note that throughout the paper we refer to 3z+Ly- $\alpha$  data for the observables, unless otherwise quoted as 9z+Ly- $\alpha$  data.

The likelihood for the correlated BAO data is implemented as,

$$\mathcal{L}_{BAO} \propto \exp \left[ (Y_{data} - Y_{th}) \cdot \Sigma_{BAO}^{-1} \cdot (Y_{data} - Y_{th})^T \right]. \quad (3.2)$$

where  $Y_{data}$  is the data described in Table 1 and the  $Y_{th}$  is the theoretical model evaluated at the respective redshifts, while  $\Sigma_{BAO}$  denotes the total covariance matrix of the BAO data for either of

---

<sup>3</sup>All values of the mean, dispersion and covariances of  $D_M\&H$  observables for the galaxy clustering BAO data are taken from <https://data.sdss.org/sas/dr12/boss/papers/clustering/>. [6] also provides the covariances for 3z  $D_V\&AP$ , while [32] provides the covariances only for 9z  $D_M\&H$ .

**Table 1.** BAO data in  $D_V\&AP$  formalism. The reference I corresponds to [6], which provides both the data and the covariances. We construct the Lyman- $\alpha$   $D_V\&AP$  data using the measurements  $D_M\&H$  from references II [29] and III [28].

$z$	$D_V/r_d$	$AP$	Reference
0.38	$9.995 \pm 0.111$	$0.413 \pm 0.013$	I
0.51	$12.700 \pm 0.129$	$0.597 \pm 0.017$	I
0.61	$14.482 \pm 0.149$	$0.741 \pm 0.021$	I
2.33	$31.123 \pm 1.087$	$4.164 \pm 0.317$	II
2.4	$30.206 \pm 0.892$	$3.962 \pm 0.288$	III

**Table 2.** For completeness we show here the total covarince matrix ( $C_{ij}$ ) in  $D_V\&AP$  basis obtained using Eq. (3.1) for the two Lyman- $\alpha$  points at  $z = 2.33$  and  $z = 2.4$ .

Measurement	$c_{ij}$			
	$D_V(2.33)$	0.	0.25571	0.
$D_V(2.4)$	0.	0.79666	0.	0.14525
$AP(2.33)$	0.25571	0.	0.10061	0.
$AP(2.4)$	0.	0.14525	0.	0.08271

the observables ( $D_V$ ,  $AP$ ,  $D_V\&AP$  and  $D_M\&H$ ). As the  $AP$  component is independent of  $r_d$ , unlike  $D_V/r_d$ , we use  $r_d \times H_0$  (hereafter  $H_0 r_d$ ) as a free parameter, instead of using A15, to compare the individual constraints obtained from these components. However, we also implement the A15 functional form to compare the results obtained from our main analysis. For this purpose, we use Eq. (2.10) with  $\Omega_b h^2 = 0.0217$  [34] and  $\Omega_\nu h^2 = 6.42 \times 10^{-4}$  [7].

### 3.2 OHD and SNIa data

The measurements of the expansion rate have been estimated using the differential age method suggested in [35], which considers pairs of passively evolving red galaxies at similar redshifts to obtain  $dz/dt$ . We use a compilation of 31 uncorrelated data points taken from [2, 3, 36–40]. A similar compilation was also implemented in [9], but also considering the  $H(z)$  measurements from BAO data.

We implement a simple likelihood function assuming all the data are uncorrelated as,

$$\mathcal{L}_{\text{OHD}} \propto \exp \left[ -\frac{1}{2} \sum_{i=1}^{31} \left( \frac{H_i - H(z_i)}{\sigma_{H_i}} \right)^2 \right]. \quad (3.3)$$

where  $\sigma_{H_i}$  is the gaussian error on the measured value of  $H_i$ .

We use the JLA supernova compilation, with the standard  $\chi^2$  analysis as is elaborated in [1]. The JLA supernova compilation implements a correction to the absolute magnitude through the empirical relation,

$$M_B^{\text{corr}} = M_B - \alpha s + \beta c, \quad (3.4)$$

where  $M_B$  is the absolute magnitude,  $s$  and  $c$  are the stretch and colour corrections for the absolute magnitude. The likelihood for the SNIa data has been defined by evaluating an intrinsic scatter of 0.108 through the use of reduced maximum likelihood method [1]. The observed distance modulus  $\mu_{obs}$  can be written as,

$$\mu_{obs} = m_B - M_B^{\text{corr}} + \alpha s - \beta c, \quad (3.5)$$

The likelihood for the SNIa data can be written as,

$$\mathcal{L}_{\text{SN}} \propto \exp \left[ \frac{(\mu_{obs} - \mu_{th})^T \cdot \text{Cov}^{-1} \cdot (\mu_{obs} - \mu_{th})}{|\text{Cov}|} \right]. \quad (3.6)$$

where  $\text{Cov}$  denotes the total covariance matrix including the correction for the host galaxy mass.

Finally, the joint analysis is performed by combining the likelihoods for these independent datasets. The likelihood for the joint analysis is given as,

$$\mathcal{L}_{\text{TOT}} = \mathcal{L}_{\text{BAO}} \mathcal{L}_{\text{OHD}} \mathcal{L}_{\text{SN}}. \quad (3.7)$$

The OHD data plays a very important role in our joint analysis as it is the only dataset capable of discerning the degeneracy between the Hubble parameter  $H_0$  and  $M_B$  for supernova data, and the degeneracy between  $H_0$  and  $r_d$  in case of BAO data. We use the Akaike information criteria (AIC) [41] and Bayesian information (BIC) [42] for model selection. The AIC and AICc (corrected for number of data points) with a second-order correction term, are written as,

$$\text{AIC} = -2 \log \mathcal{L}^{\text{max}} + 2N_p, \quad (3.8)$$

$$\text{AICc} = -2 \log \mathcal{L}^{\text{max}} + 2N_p + \frac{2N_p(N_p + 1)}{N_d - N_p - 1}, \quad (3.9)$$

where  $N_p$  is the number of parameters and  $N_d$  is the number of data points. For large  $N_d$ , the AICc value tends to AIC, while for less  $N_d$  (e.g., BAO data) it penalises the model with more parameters strongly. Similarly the BIC can be defined as,

$$\text{BIC} = -2 \log \mathcal{L}^{\text{max}} + N_p \log(N_d), \quad (3.10)$$

The model preference is estimated by evaluating  $\Delta\text{AICc}$  ( $\Delta\text{BIC}$ ) as a difference in the AICc value of the model in question to the reference model. A positive value of  $\Delta\text{AICc}$  or  $\Delta\text{BIC}$  indicates that the reference model is preferred over the model in comparison.

## 4 Results and Discussion

In this section we present the results obtained from our analysis for BAO data alone and then for the joint analysis described in the earlier sections. We also comment on the statistical evidence for a late-time acceleration phase.

### 4.1 Results from the analysis of BAO data alone

As mentioned in the earlier sections we have used the different observables ( $D_V$ ,  $AP$ ,  $D_V \& AP$  and  $D_M \& H$ ) taken from the BAO data to constrain the standard model and its extensions. In particular, we test for the agreement  $D_V$  and  $AP$  components. In Table 3, Table 4 and Table 5 we show the best-fit parameters to  $\Lambda\text{CDM}$ ,  $k\Lambda\text{CDM}$  and  $w\text{CDM}$  models using each of the four observables. Except for the  $k\Lambda\text{CDM}$  model, the  $AP$  data gives a lower value of  $\Omega_m$  for all the standard extensions considered, while the  $D_V$  measurements give higher values of the same with similar ability to constrain the mean.

In the  $\Lambda\text{CDM}$  scenario, the  $\Omega_m$  estimates obtained using  $D_V$  and  $AP$  as independent datasets show a mild tension<sup>4</sup> at  $2.1\sigma$ . However, this tension might be overestimated if the two values of  $\Omega_m$

<sup>4</sup>As the errors are asymmetric, we assume a gaussian error using the higher among them to estimate the tension.

are anti-correlated<sup>5</sup>. Therefore, we estimate a least possible tension of  $1.5\sigma$  by assuming that they are completely anti-correlated. Using the 9z+Ly- $\alpha$  data we find the  $\Omega_m$  values from  $D_V$  and  $AP$  to be  $0.356^{+0.043}_{-0.037}$  and  $0.159^{+0.041}_{-0.034}$ , respectively. Here the discrepancy is even more pronounced and they agree only at  $3.3\sigma$  considering no correlation and a least possible tension of  $2.3\sigma$  (see Figure 1). As expected, we find that using the BAO data in either the  $D_M\&H$  or  $D_V\&AP$  formalism yield very consistent results suggesting that there is no loss of information and that these two parameter spaces are equivalent (see Table 3).

**Table 3.** Fit parameters for the four different observables in  $\Lambda$ CDM model.

Data	$\Omega_m$	$H_0 r_d$ [km/s]
$AP$	$0.225^{+0.045}_{-0.040}$	-
$D_V$	$0.358^{+0.043}_{-0.038}$	$9840^{+204}_{-212}$
$D_V\&AP$	$0.285^{+0.019}_{-0.017}$	$10182 \pm 139$
$D_M\&H$	$0.288^{+0.019}_{-0.018}$	$10162 \pm 139$

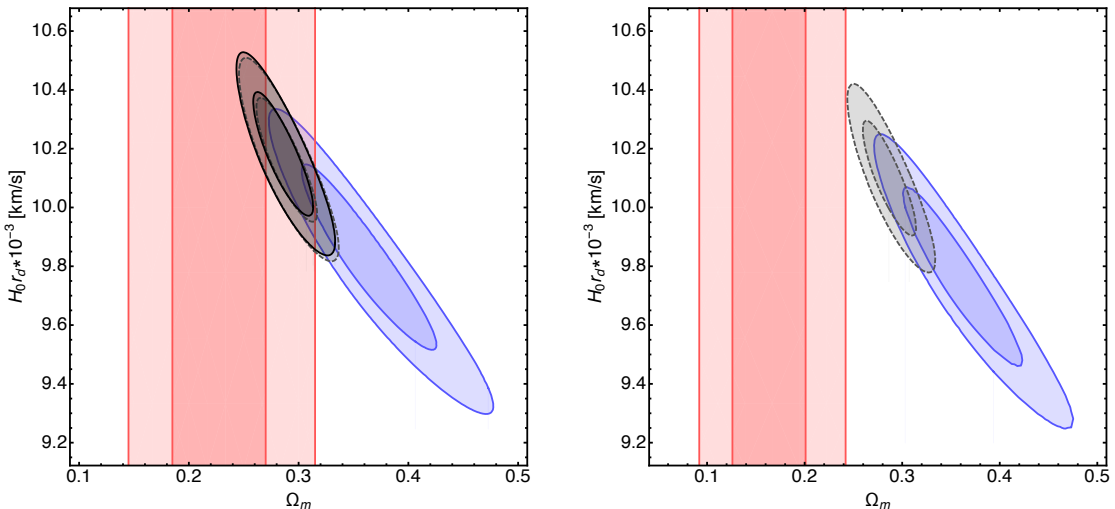


**Figure 1.** We show the 68% and 95% confidence level contours for 3z+Ly- $\alpha$  (left) and 9z+Ly- $\alpha$  (right) in  $\Lambda$ CDM scenario. The red, blue and black contours correspond to  $AP$ ,  $D_V$  and  $D_V\&AP$  methods, respectively. The gray dashed contours in both the panels shows the constraints using  $D_M\&H$  formalism.

In the  $k\Lambda$ CDM model we find that using  $AP$  data alone results in unexpected high values of  $\Omega_m$  and  $\Omega_\Lambda$  (see Figure 2). Also, a consistent estimate for the flatness in the  $k\Lambda$ CDM model can be obtained only when both  $D_V$  and  $AP$  components are used together (see left panel of Figure 2). However, using 9z+Ly- $\alpha$  data we find that the flat  $\Lambda$ CDM model is disfavoured at  $\sim 2\sigma$  (see right panel of Figure 2). In the wCDM model, we see that the ability of  $AP$  measurements to constrain the value of  $w$  is better than that of  $D_V$  measurements. Hence, the inclusion of the  $AP$  measurements is crucial to have reliable inferences, e.g., on the phantom scenario (see Figure 3). We want to stress

<sup>5</sup>It is easily verified that for positively correlated  $D_V$  and  $AP$  data, the two values of  $\Omega_m$  will be anti-correlated.

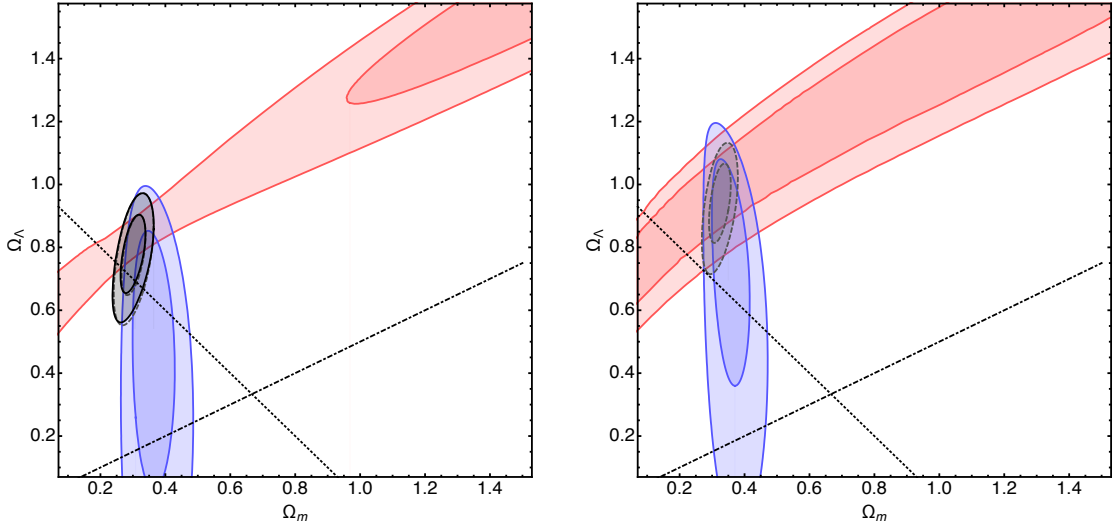


**Figure 2.** We show the 68% and 95% confidence level contours for 3z+Ly- $\alpha$  (left) and 9z+Ly- $\alpha$  (right) in  $k\Lambda$ CDM scenario. The red, blue and black contours correspond to  $AP$ ,  $D_V$  and  $D_V\&AP$  methods, respectively. The dashed contours in both the panels shows the constraints using  $D_M\&H(z)$  formalism. The dotted and the dot-dashed lines identify the flat  $\Lambda$ CDM and the transition between the accelerated and non-accelerated regimes, respectively.

**Table 4.** Best-fit parameters in the four different formalisms for  $k\Lambda$ CDM model.

Data	$\Omega_m$	$\Omega_\Lambda$	$H_0 r_d$ [km/s]
$AP$	$1.748^{+0.561}_{-0.521}$	$1.720^{+0.306}_{-0.301}$	-
$D_V$	$0.358^{+0.045}_{-0.04}$	$0.537^{+0.224}_{-0.306}$	$9632^{+504}_{-550}$
$D_V\&AP$	$0.300 \pm 0.025$	$0.786^{+0.079}_{-0.085}$	$10303^{+199}_{-199}$
$D_M\&H$	$0.302 \pm 0.024$	$0.783^{+0.081}_{-0.087}$	$10285 \pm 202$

that in all the models considered here the discrepancies between the  $D_V$  and  $AP$  constraints remain consistent from 3z to 9z data.

**Table 5.** Best-fit parameters to the BAO data in the four different methods for  $w$ CDM model.

Data	$\Omega_m$	$w$	$H_0 r_d$ [km/s]
$AP$	$0.157^{+0.062}_{-0.082}$	$-0.646^{+0.166}_{-0.174}$	-
$D_V$	$0.353^{+0.046}_{-0.104}$	$-0.822^{+0.387}_{-0.443}$	$9570^{+727}_{-551}$
$D_V\&AP$	$0.275^{+0.023}_{-0.035}$	$-0.736^{+0.166}_{-0.169}$	$9692^{+334}_{-304}$
$D_M\&H$	$0.278^{+0.024}_{-0.036}$	$-0.741^{+0.171}_{-0.174}$	$9690^{+340}_{-308}$

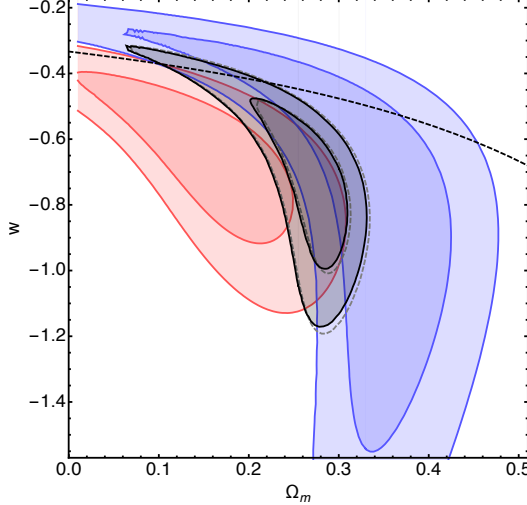


**Figure 3.** The red, blue and black contours correspond to  $AP$ ,  $D_V$  and  $D_V \& AP$  methods, respectively. We show here the 68% and 95% confidence level contours. The Dashed contours in grey show the constraints using  $D_M \& H(z)$  method. The region below (above) the dashed line corresponds to the accelerating (non-accelerating) regime.

The constraints from BAO data for the  $w_0 w_a$ CDM and the  $k w$ CDM models are discussed in the next subsection, alongside the joint analysis. Inclusion of other three BAO  $D_V$ -only points at  $z = 0.106, 0.15, 1.52$  affects the constraints from the BAO data mildly. For instance, in the  $\Lambda$ CDM model we obtain  $\Omega_m = 0.293^{+0.18}_{-0.17}$ , showing clearly the minimal effect that these data have on constraining the model. We now proceed with the joint analysis without including these three data points.

## 4.2 Joint analysis and model selection

In this section we present our constraints obtained from a joint analysis of the most recent  $D_M \& H + \text{SN} + \text{OHD}$  data. Our analysis differ from what is already present in the literature, as the BAO data are usually complemented with the CMB data. Here we don't consider the CMB data in order to test the consistency between the “low-redshift” and “high-redshift” constraints. Moreover, in order to estimate  $H_0$ , we rely on a joint analysis which includes the OHD dataset, more often not considered in this kind of analysis. In table 6 we show our findings. Note that the estimates for  $H_0$  and  $r_d$  are consistent among all the models considered here. Note also the low value of  $\Omega_m$  obtained for the  $w_0 w_a$ CDM model.

We find the best-fit estimate of  $H_0$  for the  $\Lambda$ CDM model to be  $H_0 = 69.41 \pm 1.76 \text{ km/s Mpc}^{-1}$ . Note that this value is now in the middle of the [15] ( $H_0 = 66.93 \pm 0.62 \text{ km/s Mpc}^{-1}$ ) and the R16 ( $H_0 = 73.24 \pm 1.74 \text{ km/s Mpc}^{-1}$ ) estimates, and consistent with both at  $1.33\sigma$  and  $1.55\sigma$ , respectively. However, now the three  $H_0$  estimates -from this work, P16 and R16- are at a higher total inconsistency with the IOI<sup>6</sup>  $\sim 4.2$ . In a more recent work ([45]), a combination of five independent datasets namely, CMB+DES+BAO+BBN+(SPTpol [46]) along with constraints from Sh0ES [11] and H0liCOW [47] was implemented to quote a value of  $H_0 = 69.1^{+0.4}_{-0.6} \text{ km/s Mpc}^{-1}$ , which we are in a very good agreement with. Also, our estimate on  $H_0$  which is derived by the inclusion of OHD

<sup>6</sup>Index of Inconsistency (IOI) [43, 44] was proposed to measure the inconsistency between constraints obtained from two or more different datasets. Please take a look at Eq. 11-13 of [43]. It was also shown that in the gaussian limit IOI reduces to standard tension, which is the case here.

**Table 6.** Best-fit estimates and parameter constraints using the  $D_M\&H$ +SN+OHD data.

Model	$\Omega_m$	$H_0[\text{km/s Mpc}^{-1}]$	$w_0/w$	$w_a$	$\Omega_\Lambda$	$r_d[\text{Mpc}]$
$\Lambda\text{CDM}$	$0.292^{+0.016}_{-0.015}$	$69.41 \pm 1.76$	-	-	-	$146.0^{+3.6}_{-3.4}$
$k\Lambda\text{CDM}$	$0.296 \pm 0.024$	$69.62^{+2}_{-1.98}$	-	-	$0.722^{+0.064}_{-0.067}$	$145.9^{+3.7}_{-3.5}$
$w\text{CDM}$	$0.285 \pm 0.018$	$68.61^{+1.93}_{-1.91}$	$-0.921^{+0.08}_{-0.081}$	-	-	$146.2^{+3.6}_{-3.4}$
$w_0w_a\text{CDM}$	$0.195^{+0.084}_{-0.23}$	$68.75^{+1.95}_{-1.92}$	$-0.902^{+0.222}_{-0.125}$	$0.838^{+0.217}_{-0.655}$	-	$146.5^{+3.6}_{-3.5}$
$kw\text{CDM}$	$0.311 \pm 0.025$	$69.27^{+2.0}_{-1.97}$	$-0.828^{+0.075}_{-0.089}$	-	$0.872 \pm 0.107$	$144.9^{+3.7}_{-3.5}$

dataset is very consistent with  $H_0 = 71.75 \pm 3.05 \text{ km/s Mpc}^{-1}$  quoted in [10], which was obtained using the galaxy-clustering BAO data alone.

As an attempt to resolve the tension between the P16 and R16  $H_0$  estimates, [48] have considered a 12-parameter extended CMB analysis with R16 prior together with an older BAO dataset or with the JLA data [48]. This approach clearly resolves the  $H_0$  tension and provides values for EOS parameter  $w$  consistent with our result. This suggests that for the  $w\text{CDM}$  model the low-redshift analysis performed here is perfectly consistent with the Planck data.

We find that an assumption of the approximate formula (A15) in the  $w_0w_a\text{CDM}$  model tends to improve the agreement with the standard model (see right panel of Figure 4), with  $\Omega_m = 0.302 \pm 0.016$  and  $H_0 = 67.57^{+1.68}_{-1.70} \text{ km/s Mpc}^{-1}$ . Clearly, there is a degeneracy between  $\Omega_m$  and the DE parameters ( $w_0, w_a$ ) that is removed when the A15 formula is assumed. While in the  $kw\text{CDM}$  model the approximate formulae does not show any significant influence on the constraints from joint analysis. However, the  $kw\text{CDM}$  model is in agreement with the standard model at  $1.12\sigma$  from our joint analysis, while using  $D_M\&H$  data alone shows that the standard model is in agreement only at  $2.2\sigma$  (see Figure 4). The individual priors of  $\Omega_k = 0$  in the  $w\text{CDM}$  model and  $w = -1$  in  $k\Lambda\text{CDM}$  model tend to converge their model constraints to  $\Lambda\text{CDM}$ . While, leaving both parameters free shows a marginal deviation from  $\Lambda\text{CDM}$ .

Constraints on the  $w_0w_a\text{CDM}$  model obtained from our joint analysis tend towards the first quadrant of Figure 4 (i.e.,  $w_0 > -1, w_a > 0$ ) and the standard model is consistent at  $1\sigma$ . We find that this deviation is slightly larger at  $1.5\sigma$  using  $AP$  data alone. Our results are not in immediate agreement with previous results, as the CMB data seems to disfavour the first quadrant [7]. On the same line, the analysis on  $w_0w_a\text{CDM}$  model presented in [49], using CMB and weak lensing data also suggests an exclusion of the first quadrant at  $\gtrsim 2\sigma$  confidence. This tension between CMB and BAO was also discussed by [13] and [50], both using an older compilation of BAO dataset. According to our result, this tension does not seem to change even when the newer BAO dataset is implemented in the analysis.

In Table 7 we show the values of the information criteria obtained from the joint analysis and  $D_M\&H$  data alone for the four models tested against  $\Lambda\text{CDM}$ .  $\Delta\text{AICc}$  strongly disfavour the extended models for  $D_M\&H$  data alone, while  $\Delta\text{BIC}$  strongly penalises them in the joint analysis. We find that  $w_0w_a\text{CDM}$  is disfavoured over  $\Lambda\text{CDM}$  with  $\Delta\text{BIC} = 10.9$ . The standard information criteria like BIC tend to heavily penalise models with extra parameters as the number of data points increase. In fact, [51] predicted an oscillatory nature for dark energy EOS using model-independent technique.

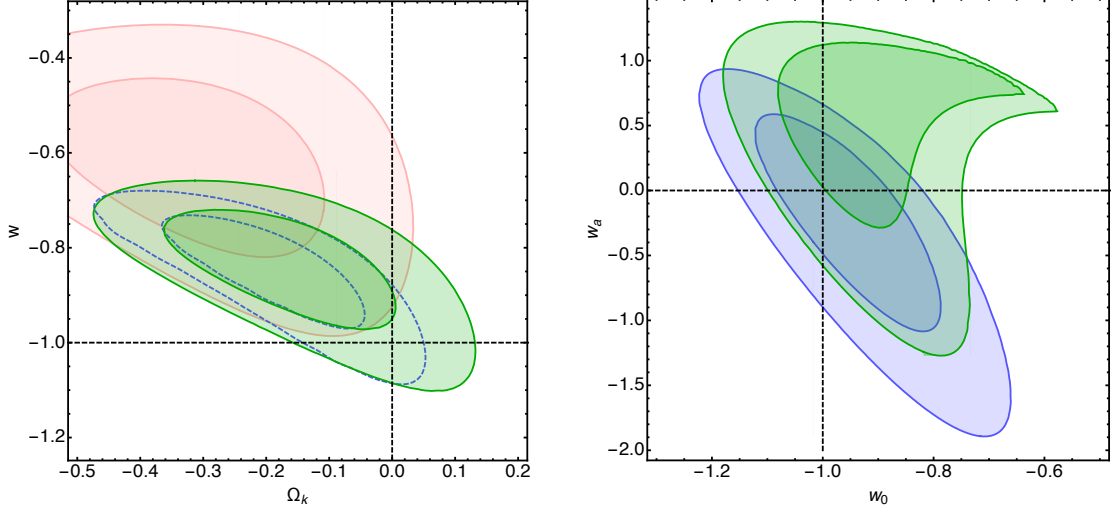


**Figure 4.** *Left panel:* Here we show the 68% and 95% confidence level contours obtained for the  $kw$ CDM model using  $D_M \& H(z)$ +SN+OHD data, with(blue) and without(green) the approximate formula A15. The intersection of the dashed lines (0, -1) correspond to the standard model. The red contours correspond to the  $kw$ CDM fit using the  $D_M \& H$  data alone. *Right Panel:* We show the 68% and 95% confidence level contours obtained for the  $w_0w_a$ CDM model using  $D_M \& H(z)$ +SN+OHD data, with(blue) and without(green) the approximate formula A15. The intersection of the dashed lines (-1, 0) correspond to the standard model.

They have quoted a  $3.5\sigma$  preference for this dynamical dark energy over  $\Lambda$ CDM using the Kullback-Leibler divergence, which the bayesian evidence is unable to provide. The CPL parametrisation was shown to be a very good approximation for a wide range of scalar field models and modified gravity scenarios in [52]. However, taking into account the discrepant results from the BAO and the CMB data one could infer that the CPL parametrisation is unable to provide conclusive evidence for dynamical nature of dark energy. This evidence should be more generally inferred for a physically motivated  $w(z)$  or through a model independent analysis instead of a simple Taylor expansion around  $a = 1$ , which is imposed over the range of data  $0.285 < a < 1$ .

**Table 7.** Comparison of the  $\Delta\text{AICc}$  and  $\Delta\text{BIC}$  criteria for the extended models with  $\Lambda$ CDM as the reference model. The first two columns correspond to the joint analysis and the last two columns are estimated from  $D_M \& H$  data alone.

Model	$\Delta\text{AICc}$	$\Delta\text{BIC}$	$\Delta\text{AICc}_{D_M \& H}$	$\Delta\text{BIC}_{D_M \& H}$
$w$ CDM	1.09	5.71	2.15	0.16
$k\Lambda$ CDM	1.20	6.61	3.58	1.60
$kw$ CDM	0.97	10.20	3.05	-2.63
$w_0w_a$ CDM	1.67	10.90	7.42	1.74

### 4.3 Comment on acceleration

SNIa observations have been the first to provide an evidence for acceleration [53, 54]. In more recent work this evidence has been questioned [17] and further discussed [18–21]. However, the

recent BAO data is now capable of constraining the acceleration with much higher significance. In an earlier work, [22] have quoted an evidence of  $6.5\sigma$  using the BAO data alone. In the  $k\Lambda$ CDM scenario, using the  $D_M \& H$  data, we find, in agreement with [22], that the acceleration is significant at  $5.8\sigma$ . It is important to note that the evidence for acceleration obtained using the BAO data is coming from the  $AP$  component. In fact using  $AP$  alone, we find that acceleration is preferred at  $6.0\sigma$ . Also, from  $9z+Ly-\alpha$  data we have this evidence at  $6.6\sigma$ . On the contrary, the  $D_V$  component is incapable of constraining the acceleration, while it constraints  $\Omega_m$  extremely well (see Figure 2). The evidence for the late-time acceleration increases when a joint analysis is performed: in the  $k\Lambda$ CDM scenario, we obtain a significance of  $8.4\sigma$ . On the other hand, BAO data unlike SNIa is unable to provide a significant evidence for acceleration in the  $w$ CDM model (see Figure 2).

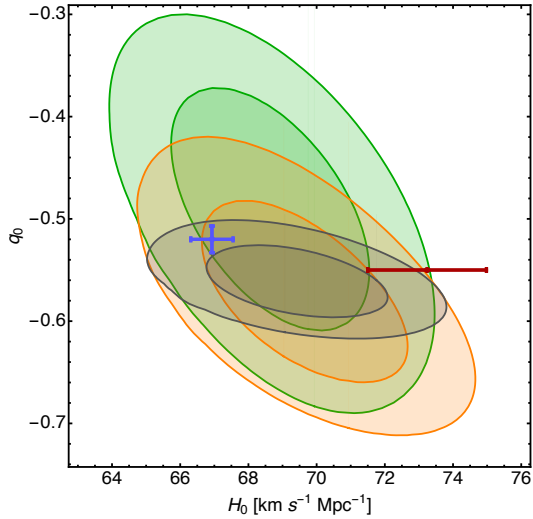


**Figure 5.** Here we show the  $q_0$  vs  $H_0$  plots for three different models. The green, orange and grey contours are shown for  $w$ CDM,  $k\Lambda$ CDM and  $\Lambda$ CDM, respectively. All contours are made using  $D_M \& H + \text{SN} + \text{OHD}$ . In blue we show the Planck constraints [15] and Riess  $H_0$  in red.

In Figure 5 we show the  $H_0 - q_0$  plane, where the significance of acceleration and the  $H_0$  estimates can be compared simultaneously. We find that all the models predict very consistent  $H_0$  and  $q_0$  values, while  $w$ CDM model shows the least evidence for an accelerated scenario.

#### 4.4 Analysis on mock data

We implement a mock dataset with Euclid-like (see Table VI. of [55]) precision built around our best-fit  $kw$ CDM model ( $\Omega_m = 0.3$ ,  $\Omega_\Lambda = 1.0$ ,  $w = -0.6$ ,  $H_0 r_d = 9610$ ) obtained using  $D_M \& H$  data alone. We fit the  $AP$  and  $D_V$  components of the mock data separately to emphasise the role of their disagreement for model selection. When we fit these two components to  $\Lambda$ CDM model, the corresponding values of  $\Omega_m$  are in a strong tension, at  $6.4\sigma$  (see top-left panel of Figure 6). Likewise, fitting  $k\Lambda$ CDM model also shows a strong disagreement as can be seen in the top-right panel of Figure 6. As expected, once we use the  $kw$ CDM model, we find a good agreement in the constraints obtained from the  $AP$  and  $D_V$  components both of which contain the “true” model (see bottom panel of Figure 6). Note, that the  $w$  parameter is better constrained by  $AP$  rather than by  $D_V$ .

The ability of the  $AP$  and  $D_V$  data to provide model selection can also be complemented by the standard information criteria. In fact, the latter indicates a clear preference for the “true” model (see Table 8). However, when the “true” model is unknown, even an insignificant evidence for model

selection based on standard information criteria can be increased by comparing the  $AP$  and  $D_V$  constraints. For example, according to standard information criteria,  $w$ CDM and  $w_0w_a$ CDM models perform as well as  $\Lambda$ CDM, even if none of them is the “true” model. The  $k\Lambda$ CDM model is clearly preferred over the previous three models with  $\Delta BIC \sim 50$ . However, the top-right panel shows that the  $AP$  and  $D_V$  strongly disagree. Finally, the  $kw$ CDM is performing better than  $k\Lambda$ CDM, both using the  $\Delta BIC \sim 15$ , and  $AP$  and  $D_V$ . So, an inspection of the  $D_V$  and  $AP$  constraints can provide a very useful guideline for model selection even without knowing the true model, as both these components are obtained from same dataset and do not have different systematics.

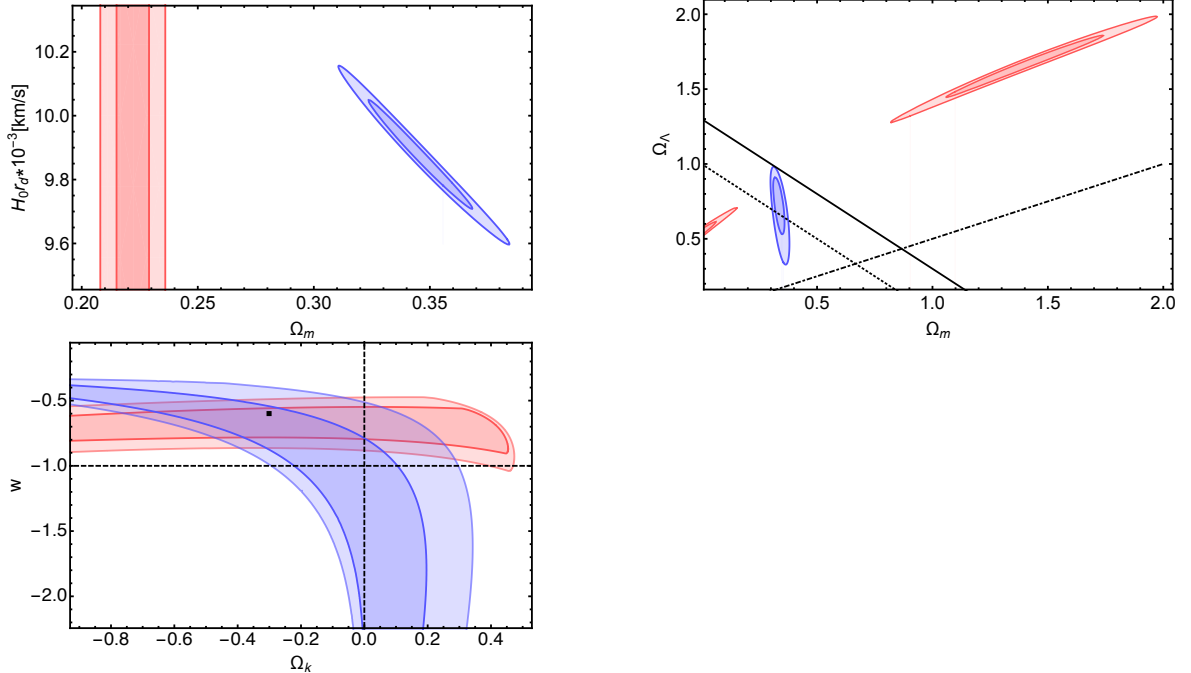


**Figure 6.** In the top-left panel we show the constraints obtained for the  $\Lambda$ CDM model from our mock dataset using the  $D_V$  (blue) and the  $AP$  (red) components separately. Similarly, we show the constraints in  $k\Lambda$ CDM (middle panel) and  $kw$ CDM (lower panel) scenario. The solid line in the middle panel corresponds to curvature of the model of the mock dataset ( $\Omega_k = -0.3$ ). The dotted line in the middle panel correspond to the flat model, the dot-dashed line marks the transition between the accelerated and non-accelerated regimes. In bottom panel the square marks the “true” model around which the mock data has been constructed and the dashed lines show the standard model.

## 5 Conclusions

In this work we have explored how different components of the BAO data constrain cosmological parameters. We find that the isotropic  $D_V$  and the anisotropic  $AP$  components can provide different constraints when used separately. We find a least possible tension of  $1.5\sigma$  for the  $\Omega_m$  values estimated in the  $\Lambda$ CDM scenario, which increases to  $2.3\sigma$  when the 9z data is used. Although, the current discrepancies are not very significant, similar comparison can be utilised to falsify cosmological models with more precise data to come from future experiments such as EUCLID [56] and DESI [57, 58]. Such a method could be utilised to circumvent the problem of possible systematics in the data. We also present an analysis of a mock scenario with Euclid-like precision [55] in which we show how these conclusions can be useful to derive significant inferences from forthcoming data.

**Table 8.** Comparison of the  $\Delta\text{AICc}$  and  $\Delta\text{BIC}$  criteria for the extended models with  $\Lambda\text{CDM}$  as the reference model. The first two columns correspond to the joint analysis and the last two columns are estimated from  $D_M\&H$  data alone.

Model	$\Delta\text{AICc}_{D_M\&H}$	$\Delta\text{BIC}_{D_M\&H}$
$w\text{CDM}$	0.68	1.60
$k\Lambda\text{CDM}$	-55.10	-54.17
$kw\text{CDM}$	-69.42	-67.77
$w_0w_a\text{CDM}$	2.70	4.34

From our joint analysis, we find  $H_0 = 69.41 \pm 1.76 \text{ km/s Mpc}^{-1}$ , which is now consistent with both Planck and R16 at  $1.33\sigma$  and  $1.55\sigma$ , respectively. Our findings also very well agree with the most stringent constraint of  $69.1_{-0.6}^{+0.4}$  quoted in [45]. However, in the  $\Lambda\text{CDM}$  scenario, the three independent  $H_0$  estimates from “low-redshift” data in this work, “high-redshift” P16 and local R16, which are at a combined tension of  $4.2\sigma$ , increase the difficulty to have a concordance value for  $H_0$ . Using BAO data in the  $D_V$  observable alone can give rise to strict constraints on  $\Omega_m$ , but not on the cosmic dynamics. This could give the impression that the BAO data is incapable of constraining acceleration. On the contrary,  $AP$  provides strong constraints on the acceleration. In fact, the evidence for acceleration is now very strong, at  $\sim 5.8\sigma$  from the BAO data alone, and reconfirms the findings from the SNIa data. Using SNIa, OHD and BAO data this evidence is found to be  $8.4\sigma$ .

In the  $kw\text{CDM}$  scenario, using  $D_M\&H$  data alone, we find a mild deviation of  $2.2\sigma$  from the standard model. Also in this case, with a  $\Delta\text{BIC} = -2.34$  the  $kw\text{CDM}$  model is preferred over  $\Lambda\text{CDM}$ . Using the CPL parameterisation we find no evidence for dynamical nature of dark energy from our joint analysis. Although, the BAO data is now providing much better constraints, the dynamical nature of dark energy still eludes in the standard methods for model selection. We also compared the constraints obtained with and without using the A15 approximate formula for the estimation of  $r_d$  in 2-parameter extended models. We find a mild difference for the  $w_0w_a\text{CDM}$  model in this comparison.

## References

- [1] M. Betoule, R. Kessler, J. Guy, J. Mosher, D. Hardin, R. Biswas et al., *Improved cosmological constraints from a joint analysis of the SDSS-II and SNLS supernova samples*, *Astron. Astrophys.* **568** (Aug., 2014) A22, [[1401.4064](#)].
- [2] J. Simon, L. Verde and R. Jimenez, *Constraints on the redshift dependence of the dark energy potential*, *Phys. Rev. D* **71** (June, 2005) 123001, [[astro-ph/0412269](#)].
- [3] M. Moresco, L. Pozzetti, A. Cimatti, R. Jimenez, C. Maraston, L. Verde et al., *A 6% measurement of the hubble parameter at  $z \sim 0.45$ : direct evidence of the epoch of cosmic re-acceleration*, *J. Cosmology Astropart. Phys.* (2016) , [[1601.01701v2](#)].
- [4] M. Moresco, L. Verde, L. Pozzetti, R. Jimenez and A. Cimatti, *New constraints on cosmological parameters and neutrino properties using the expansion rate of the Universe to  $z \sim 1.75$* , *J. Cosmology Astropart. Phys.* **7** (July, 2012) 053, [[1201.6658](#)].
- [5] D. J. Eisenstein, I. Zehavi, D. W. Hogg, R. Scoccimarro, M. R. Blanton, R. C. Nichol et al., *Detection of the Baryon Acoustic Peak in the Large-Scale Correlation Function of SDSS Luminous Red Galaxies*, *Astrophys. J.* **633** (Nov., 2005) 560–574, [[astro-ph/0501171](#)].

- [6] S. Alam, M. Ata, S. Bailey, F. Beutler, D. Bizyaev, J. A. Blazek et al., *The clustering of galaxies in the completed SDSS-III Baryon Oscillation Spectroscopic Survey: cosmological analysis of the DR12 galaxy sample*, *arXiv preprint arXiv:1607.03155* (2016) .
- [7] P. Ade, N. Aghanim, M. Arnaud, M. Ashdown, J. Aumont, C. Baccigalupi et al., *Planck 2015 results-XIII. cosmological parameters*, *Astron. Astrophys.* **594** (2016) A13.
- [8] É. Aubourg, S. Bailey, J. E. Bautista, F. Beutler, V. Bhardwaj, D. Bizyaev et al., *Cosmological implications of baryon acoustic oscillation measurements*, *Phys. Rev. D* **92** (Dec., 2015) 123516, [[1411.1074](#)].
- [9] O. Farooq, F. R. Madiyar, S. Crandall and B. Ratra, *Hubble parameter measurement constraints on the redshift of the deceleration-acceleration transition, dynamical dark energy, and space curvature*, *Astrophys. J.* **835** (2017) 26, [[1607.03537](#)].
- [10] Y. Wang, L. Xu and G.-B. Zhao, *A measurement of the hubble constant using galaxy redshift surveys*, *ArXiv e-prints* (June, 2017) , [[1706.09149](#)].
- [11] A. G. Riess, L. M. Macri, S. L. Hoffmann, D. Scolnic, S. Casertano, A. V. Filippenko et al., *A 2.4% determination of the local value of the hubble constant*, *Astrophys. J.* **826** (July, 2016) 56, [[1604.01424](#)].
- [12] V. V. Luković, R. D'Agostino and N. Vittorio, *Is there a concordance value for  $H_0$ ?*, *Astron. Astrophys.* **595** (Nov., 2016) A109, [[1607.05677](#)].
- [13] J. L. Bernal, L. Verde and A. G. Riess, *The trouble with  $H_0$* , *J. Cosmology Astropart. Phys.* **2016** (2016) 019.
- [14] R. I. Anderson and A. G. Riess, *On cepheid distance scale bias due to stellar companions and cluster populations*, *ArXiv e-prints* (Dec., 2017) , [[1712.01065](#)].
- [15] Planck Collaboration, N. Aghanim, M. Ashdown, J. Aumont, C. Baccigalupi, M. Ballardini et al., *Planck intermediate results. XLVI. reduction of large-scale systematic effects in HFI polarization maps and estimation of the reionization optical depth*, *Astron. Astrophys.* **596** (Dec., 2016) A107, [[1605.02985](#)].
- [16] G. E. Addison, D. J. Watts, C. L. Bennett, M. Halpern, G. Hinshaw and J. L. Weiland, *Elucidating  $\Lambda$ CDM: Impact of Baryon Acoustic Oscillation Measurements on the Hubble Constant Discrepancy*, *ArXiv e-prints* (July, 2017) , [[1707.06547](#)].
- [17] J. T. Nielsen, A. Guffanti and S. Sarkar, *Marginal evidence for cosmic acceleration from Type Ia supernovae*, *Scientific Reports* **6** (Oct., 2016) 35596, [[1506.01354](#)].
- [18] D. Rubin and B. Hayden, *Is the Expansion of the Universe Accelerating? All Signs Point to Yes*, *Astrophys. J. Lett.* **833** (Dec., 2016) L30, [[1610.08972](#)].
- [19] B. S. Haridasu, V. V. Luković, R. D'Agostino and N. Vittorio, *Strong evidence for an accelerating universe*, *Astron. Astrophys.* **600** (Apr., 2017) L1, [[1702.08244](#)].
- [20] I. Tutusaus, B. Lamine, A. Dupays and A. Blanchard, *Is cosmic acceleration proven by local cosmological probes?*, *Astron. Astrophys.* **602** (June, 2017) A73, [[1706.05036](#)].
- [21] L. H. Dam, A. Heinesen and D. L. Wiltshire, *Apparent cosmic acceleration from Type Ia supernovae*, *Mon. Not. Roy. Astron. Soc.* **472** (Nov., 2017) 835–851, [[1706.07236](#)].
- [22] M. Ata, F. Baumgarten, J. Bautista, F. Beutler, D. Bizyaev, M. R. Blanton et al., *The clustering of the SDSS-IV extended Baryon Oscillation Spectroscopic Survey DR14 quasar sample: First measurement of Baryon Acoustic Oscillations between redshift 0.8 and 2.2*, *ArXiv e-prints* (May, 2017) , [[1705.06373](#)].
- [23] C. Alcock and B. Paczyński, *An evolution free test for non-zero cosmological constant*, *Nature* **281** (1979) 358–359.
- [24] M. Chevallier and D. Polarski, *Accelerating universes with scaling dark matter*, *International Journal of Modern Physics D* **10** (2001) 213–223, [[gr-qc/0009008](#)].

- [25] E. V. Linder, *Exploring the expansion history of the universe*, *Physical Review Letters* **90** (Mar., 2003) 091301, [[astro-ph/0208512](#)].
- [26] T. Delubac, J. E. Bautista, N. G. Busca, J. Rich, D. Kirkby, S. Bailey et al., *Baryon acoustic oscillations in the Ly $\alpha$  forest of BOSS DR11 quasars*, *Astron. Astrophys.* **574** (Feb., 2015) A59, [[1404.1801](#)].
- [27] A. Font-Ribera, D. Kirkby, N. Busca, J. Miralda-Escudé, N. P. Ross, A. Slosar et al., *Quasar-Lyman  $\alpha$  forest cross-correlation from BOSS DR11: Baryon Acoustic Oscillations*, *J. Cosmology Astropart. Phys.* **5** (May, 2014) 27, [[1311.1767](#)].
- [28] H. du Mas des Bourboux, J.-M. L. Goff, M. Blomqvist, N. G. Busca, J. Guy, J. Rich et al., *Baryon acoustic oscillations from the complete SDSS-III Ly-quasar cross-correlation function at  $z = 2.4$* , [1708.02225v1](#).
- [29] J. E. Bautista, N. G. Busca, J. Guy, J. Rich, M. Blomqvist, H. du Mas des Bourboux et al., *Measurement of baryon acoustic oscillation correlations at  $z = 2.3$  with SDSS DR12 Ly $\alpha$ -Forests*, *Astron. Astrophys.* **603** (June, 2017) A12, [[1702.00176](#)].
- [30] F. Beutler, C. Blake, M. Colless, D. H. Jones, L. Staveley-Smith, L. Campbell et al., *The 6dF Galaxy Survey: baryon acoustic oscillations and the local Hubble constant*, *Mon. Not. Roy. Astron. Soc.* **416** (Oct., 2011) 3017–3032, [[1106.3366](#)].
- [31] A. J. Ross, L. Samushia, C. Howlett, W. J. Percival, A. Burden and M. Manera, *The clustering of the SDSS DR7 main Galaxy sample - I. A 4 per cent distance measure at  $z = 0.15$* , *Mon. Not. Roy. Astron. Soc.* **449** (May, 2015) 835–847, [[1409.3242](#)].
- [32] G.-B. Zhao, Y. Wang, S. Saito, D. Wang, A. J. Ross, F. Beutler et al., *The clustering of galaxies in the completed SDSS-III Baryon Oscillation Spectroscopic Survey: tomographic BAO analysis of DR12 combined sample in Fourier space*, *Mon. Not. Roy. Astron. Soc.* **466** (2016) 762–779.
- [33] Y. Wang, G.-B. Zhao, C.-H. Chuang, A. J. Ross, W. J. Percival, H. Gil-Marín et al., *The clustering of galaxies in the completed SDSS-III Baryon Oscillation Spectroscopic Survey: tomographic BAO analysis of DR12 combined sample in configuration space*, *Mon. Not. Roy. Astron. Soc.* **469** (2017) 3762–3774.
- [34] S. Riemer-Sørensen and E. Sem Jønsson, *Nucleosynthesis predictions and high-precision deuterium measurements*, *ArXiv e-prints* (May, 2017) , [[1705.03653](#)].
- [35] R. Jimenez and A. Loeb, *Constraining Cosmological Parameters Based on Relative Galaxy Ages*, *Astrophys. J.* **573** (July, 2002) 37–42, [[astro-ph/0106145](#)].
- [36] D. Stern, R. Jimenez, L. Verde, S. A. Stanford and M. Kamionkowski, *Cosmic chronometers: Constraining the equation of state of dark energy. ii. a spectroscopic catalog of red galaxies in galaxy clusters*, *Astrophys. J. S* **188** (May, 2010) 280–289, [[0907.3152](#)].
- [37] M. Moresco, A. Cimatti, R. Jimenez, L. Pozzetti, G. Zamorani, M. Bolzonella et al., *Improved constraints on the expansion rate of the Universe up to  $z \sim 1.1$  from the spectroscopic evolution of cosmic chronometers*, *J. Cosmology Astropart. Phys.* **8** (Aug., 2012) 006, [[1201.3609](#)].
- [38] M. Moresco, *Raising the bar: new constraints on the Hubble parameter with cosmic chronometers at  $z \sim 2$* , *Mon. Not. Roy. Astron. Soc.* **450** (June, 2015) L16–L20, [[1503.01116](#)].
- [39] C. Zhang, H. Zhang, S. Yuan, S. Liu, T.-J. Zhang and Y.-C. Sun, *Four new observational  $H(z)$  data from luminous red galaxies in the Sloan Digital Sky Survey data release seven*, *Research in Astronomy and Astrophysics* **14** (Oct., 2014) 1221–1233, [[1207.4541](#)].
- [40] A. L. Ratsimbazafy, S. I. Loubser, S. M. Crawford, C. M. Cress, B. A. Bassett, R. C. Nichol et al., *Age-dating luminous red galaxies observed with the southern african large telescope*, *Mon. Not. Roy. Astron. Soc.* **467** (May, 2017) 3239–3254, [[1702.00418](#)].
- [41] H. Akaike, *A New Look at the Statistical Model Identification*, *IEEE Transactions on Automatic Control* **19** (1974) 716–723.

- [42] G. Schwarz et al., *Estimating the dimension of a model*, *The annals of statistics* **6** (1978) 461–464.
- [43] W. Lin and M. Ishak, *Cosmological discordances: A new measure, marginalization effects, and application to geometry versus growth current data sets*, *Phys. Rev. D* **96** (July, 2017) 023532, [[1705.05303](#)].
- [44] W. Lin and M. Ishak, *Cosmological discordances. ii. hubble constant, planck and large-scale-structure data sets*, *Phys. Rev. D* **96** (Oct., 2017) 083532, [[1708.09813](#)].
- [45] DES Collaboration, T. M. C. Abbott, F. B. Abdalla, J. Annis, K. Bechtol, B. A. Benson et al., *Dark energy survey year 1 results: A precise  $H_0$  measurement from DES Y1, BAO, and D/H Data*, *ArXiv e-prints* (2017) , [[1711.00403v1](#)].
- [46] J. W. Henning, J. T. Sayre, C. L. Reichardt, P. A. R. Ade, A. J. Anderson, J. E. Austermann et al., *Measurements of the temperature and e-mode polarization of the cmb from 500 square degrees of sptpol data*, *ArXiv e-prints* (2017) , [[1707.09353v2](#)].
- [47] V. Bonvin, F. Courbin, S. H. Suyu, P. J. Marshall, C. E. Rusu, D. Sluse et al., *HOLiCOW - V. New COSMOGRAIL time delays of HE 0435-1223:  $H_0$  to 3.8 per cent precision from strong lensing in a flat  $\Lambda$ CDM model*, *Mon. Not. Roy. Astron. Soc.* **465** (Mar., 2017) 4914–4930, [[1607.01790](#)].
- [48] E. Di Valentino, A. Melchiorri and J. Silk, *Reconciling planck with the local value of  $h_0$  in extended parameter space*, *Physics Letters B* **761** (Oct., 2016) 242–246, [[1606.00634](#)].
- [49] S. Joudaki, A. Mead, C. Blake, A. Choi, J. de Jong, T. Erben et al., *Kids-450: testing extensions to the standard cosmological model*, *Mon. Not. Roy. Astron. Soc.* **471** (Oct., 2017) 1259–1279, [[1610.04606](#)].
- [50] E. Di Valentino, A. Melchiorri, E. V. Linder and J. Silk, *Constraining dark energy dynamics in extended parameter space*, *Phys. Rev. D* **96** (July, 2017) 023523, [[1704.00762](#)].
- [51] G.-B. Zhao, M. Raveri, L. Pogosian, Y. Wang, R. G. Crittenden, W. J. Handley et al., *Dynamical dark energy in light of the latest observations*, *Nature Astronomy* **1** (Sept., 2017) 627–632, [[1701.08165](#)].
- [52] E. V. Linder, *Quintessence's last stand?*, [1501.01634v1](#).
- [53] A. G. Riess, A. V. Filippenko, P. Challis, A. Clocchiatti, A. Diercks, P. M. Garnavich et al., *Observational Evidence from Supernovae for an Accelerating Universe and a Cosmological Constant*, *AJ* **116** (Sept., 1998) 1009–1038, [[astro-ph/9805201](#)].
- [54] S. Perlmutter, G. Aldering, G. Goldhaber, R. A. Knop, P. Nugent, P. G. Castro et al., *Measurements of  $\Omega$  and  $\Lambda$  from 42 High-Redshift Supernovae*, *Astrophys. J.* **517** (June, 1999) 565–586, [[astro-ph/9812133](#)].
- [55] A. Font-Ribera, P. McDonald, N. Mostek, B. A. Reid, H.-J. Seo and A. Slosar, *Desi and other dark energy experiments in the era of neutrino mass measurements*, *ArXiv e-prints* (2013) , [[1308.4164v2](#)].
- [56] R. Laureijs, J. Amiaux, S. Arduini, J. . Auguères, J. Brinchmann, R. Cole et al., *Euclid definition study report*, *ArXiv e-prints* (Oct., 2011) , [[1110.3193](#)].
- [57] D. Collaboration, A. Aghamousa, J. Aguilar, S. Ahlen, S. Alam, L. E. Allen et al., *The DESI Experiment Part I: Science, targeting, and survey design*, *ArXiv e-prints* (Oct., 2016) , [[1611.00036](#)].
- [58] D. Collaboration, A. Aghamousa, J. Aguilar, S. Ahlen, S. Alam, L. E. Allen et al., *The DESI Experiment Part II: Instrument design*, *ArXiv e-prints* (Oct., 2016) , [[1611.00037](#)].